Available online at website: https://journal.bcrec.id/index.php/bcrec

Bulletin of Chemical Reaction Engineering & Catalysis, 20 (1) 2025, 89-98

Research Article

Catalytic Performance of Cu-Ni supported on Rice Husk Ash-derived SiO2 for the Hydrogenation of Ethylene Carbonate to Ethylene Glycol

Najiah Sephia Maharani[1,2], Novia Dwi Rahmawati[1,2], Isalmi Aziz[2], Yati Maryati[1], Egi Agustian[1], Robert Ronal Widjaya[1], Indri Yati[1], Joni Prasetyo[1], Nino Rinaldi[1], Adid Adep Dwiatmoko[1,*]

[1]Research Center for Chemistry, National Research and Innovation Agency (BRIN), Tangerang Selatan, Indonesia
[2]Department of Chemistry, Faculty of Science and Technology, UIN Syarif Hidayatullah, Tangerang Selatan, Indonesia.

Received: 31th December 2024; Revised: 6th February 2025; Accepted: 6th February 2025
Available online: 8th February 2025; Published regularly: April 2025

Abstract

Ethylene glycol, a crucial compound extensively utilized in solvents, coolants, antifreeze, polyester fiber production, and as a natural gas-drying agent, can be synthesized via the hydrogenation of ethylene carbonate. In this study, the synthesis, characterization, and catalytic performance of Cu-Ni/SiO_2 catalysts for this reaction, utilizing silica (SiO_2) derived from rice husk ash, were investigated. Silica was impregnated with copper (Cu) and nickel (Ni) by varying the weight ratio (Cu:Ni = 10, 7:3, 3:7, 10) to prepare bimetallic catalysts. X-ray Diffraction (XRD) analysis confirmed the presence of both Cu and Ni phases in all the catalysts. The 3Cu7Ni/SiO_2 catalyst displayed the lowest reduction temperature and the largest surface area (257.97 m^2/g). The 7Cu3Ni/SiO_2 catalyst exhibited the highest acidity (1.91 mmol/g) and superior metal dispersion, as confirmed by the Field Emission Scanning Electron Microscopy - Energy Dispersive X-Ray (FE-SEM-EDX) analysis. Catalytic activity was evaluated in a batch reactor under 40 bar H_2 pressure at 150 °C for 3 h with a catalyst-to-ethylene carbonate ratio of 5:1. Among the catalysts examined, the 7Cu3Ni/SiO_2 composition demonstrated the highest catalytic performance, achieving 15.14% conversion of ethylene carbonate and 80.51% selectivity towards ethylene glycol.

Keywords: Bimetallic Catalysts; Ethylene Carbonate; Ethylene Glycol; Hydrogenation; Silica

How to Cite: Maharani, N. S., Rahmawati, N. D., Aziz, I., Maryati, Y., Agustian, E., Widjaya, R. R., Yati, I., Prasetyo, J., Rinaldi, N., Dwiatmoko, A. A. (2025). Catalytic Performance of Cu-Ni supported on Rice Husk Ash-derived SiO2 for the Hydrogenation of Ethylene Carbonate to Ethylene Glycol. *Bulletin of Chemical Reaction Engineering & Catalysis*, 20 (1), 89-98. (doi: 10.9767/bcrec.20336)

Permalink/DOI: https://doi.org/10.9767/bcrec.20336

1. Introduction

Ethylene glycol has numerous applications as a solvent, engine coolant, antifreeze in vehicle radiators, polyester fibers, resins, and drying agents for natural gas production [1]. Traditionally, it is synthesized via non-catalytic hydration of ethylene oxide; however, this process requires large amounts of water, high energy consumption, and expensive evaporation steps [2]. Ethylene carbonate is an alternative feedstock that can be hydrogenated to produce ethylene glycol, offering an environmentally friendly, cost-effective, and simple process [3]. Cu-based catalysts have been widely studied for this reaction [3,4].

Silica (SiO_2), widely available in Indonesia as rice husk, is a cost-effective catalyst support [5]. SiO_2 is extracted by converting rice husks into silica-rich ash, followed by treatment with acids or alkalis [6]. Several studies have used silica-supported catalysts for ethylene glycol production [3,4,7–10].

* Corresponding Author.
Email: adid001@brin.go.id (A. A. Dwiatmoko)

Bimetallic catalysts are known to enhance the reactivity and selectivity of various catalytic processes because of the synergistic effect between the two metals. These catalysts allow for tailored electronic and geometric properties, leading to improved reaction performance [11]. For example, the addition of Pt to Cu/SiO_2 enhances the catalytic properties of Cu by lowering the H_2/ethylene carbonate molar ratio, promoting the reducibility and dispersion of Cu, and enhancing the surface density of Cu^+ species [12]. This enhancement is attributed to the strong interaction between Cu and Pt, which leads to the formation of alloyed Pt single-atoms on the Cu lattice. In addition, the addition of small amounts of Ni can enhance Cu dispersion and increase the presence of surface Cu^+ species, owing to the strong interaction between the Cu and Ni components [10]. Furthermore, it can lead to the formation of evenly distributed Cu-Ni alloy particles, which improve the adsorption and breakdown of H_2.

This study aims to synthesize Cu-Ni/SiO catalysts with different metal ratios (Cu:Ni = 10:0, 7:3, 3:7, and 0:10) using rice husk-derived silica as a support to determine the synergistic effects between Cu and Ni in bimetallic catalysts. The catalysts were characterized using Field Emission Scanning Electron Microscopy - Energy Dispersive X-Ray (FE-SEM-EDX), Transmission Electron Microscope (TEM), N_2-physisorption, X-ray Fluorescence (XRF), X-ray Diffraction (XRD), H_2 Temperature Programmed Reduction (H_2-TPR), and NH_3 Temperature Programmed Desorption (NH_3-TPD). The catalytic activity was tested via the hydrogenation of ethylene carbonate in a batch reactor at 40 bar H_2 pressure and 150 °C for 3 h. The results were analyzed using GC-FID to determine the ethylene carbonate conversion and selectivity and to identify the optimal catalyst ratio.

2. Materials and Methods

2.1 Materials

Copper(II) nitrate trihydrate ($Cu(NO_3)_2.3H_2O$), sulfuric acid (95-97%), sodium hydroxide, 2-propanol, and nickel(II) nitrate hexahydrate ($Ni(NO_3)_2.6H_2O$) were supplied by Merck. Ethylene carbonate was obtained from TCI. Hydrochloric acid (37%) obtained from Smartlab.

2.2 Catalyst Preparations

Rice husk samples were calcined in a furnace at 650 °C for 4 h at a heating rate of 20 °C/min. The product was pulverized using a mortar and sieved through a 75 μm sieve. Next, 20 g of rice husk ash was added to 200 mL of 6 N HCl solution and soaked for 1 h, followed by stirring for 2 h. The mixture was filtered using Whatman No.41 filter paper, and the residue obtained was rinsed using distilled water and then dried in an oven at 110 °C for 12 h. The sample was then dissolved in 160 mL of 2.5 N NaOH solution and heated at 90 °C for 3 h with constant stirring. The filtrate was again filtered to obtain a clear filtrate, which H_2SO_4 was then added to the filtrate solution with constant stirring under controlled conditions until a silica gel was formed. The silica gel was filtered, washed using warm distilled water, and dried at 110 °C for 12 h.

$Cu(NO_3)_2.3H_2O$ and $Ni(NO_3)_2.6H_2O$ were weighed in Cu:Ni ratios of 10:0, 7:3, 3:7, and 0:10 to achieve a total metal loading of 10 wt.% in the catalyst, placed into a 250 mL beaker, and then 80 mL of distilled water was added and stirred until dissolution. Then, 3.6 g of SiO_2 support was added, and the solution was stirred for 3 h. The solution was sonicated at 40 °C for 1 h. The solvent was evaporated at 90 °C until a solid was obtained. The solid was then transferred to a porcelain cup and dried in an oven at 120 °C for 12 h. The solid was crushed and calcined in a furnace at 500 °C for 3 h. Subsequently, reduction using H_2 gas was performed in a tubular furnace at 550 °C for 4 h.

2.3 Catalyst Characterizations

The crystal structure of the catalyst was analyzed using X-ray diffraction (Rigaku SmartLab) with Cu-Kα radiation at a voltage of 45 kV and current of 40 m, with a measurement angle range of 5–90º. The elemental compositions of the catalysts were analyzed by X-ray fluorescence (Bruker S2 PUMA). Ammonia Temperature-Programmed Desorption (NH_3-TPD) was performed to assess the acidity of the catalysts (AutoChem II). Prior to adsorption, the catalyst was heated to 350 °C for 60 min under a stream of inert helium (He) gas. The adsorption of NH_3 (5% in He, v/v) was performed at 100 °C for 30 min, followed by purging with helium gas at the same temperature for 30 min. The desorption of NH_3 was performed over a temperature range of 100–800 °C at a heating rate of 10 °C/min. To quantify the total acidity, a calibration curve was established by injecting known amounts of NH_3 gas (1, 2, 3, 4%, and 5% in He, v/v) and measuring the corresponding TCD signal. The area under the NH_3 desorption peak from the catalyst was integrated and compared with the calibration curve to determine the total acidity, expressed as mmol NH_3/g catalyst [13,14]. The surface area of the catalyst was determined using the Brunauer–Emmett–Teller (BET) method (Micromeritics TriStar II 3020), and the pore diameter and volume were analyzed using the Barrett–Joyner (BJH) method. The H_2-TPR catalyst was used to determine the reducibility of the catalyst

(AutoChem II). First, the catalyst was heated at 200 °C for 1 h under inert gas. The reduction was performed with H_2 gas (5% in Ar, v/v) over a temperature range of room temperature to 800 °C, with a temperature increase of 10 °C/min. Field-emission scanning electron microscopy (FE-SEM) was performed using Jeol JIB-4610F to determine the morphology and elements.

2.4 Catalytic Reactions

The hydrogenation of ethylene carbonate was performed in a 100 mL batch reactor. First, ethylene carbonate (0.5 g) was dissolved in 20 mL of 2-propanol, mixed with 0.1 g catalyst and placed in a batch reactor. The reactor was tightly closed and H_2 gas was purged three times to remove air and then with H_2 gas at a pressure of 40 bar. The reaction was carried out at 150 °C for 3 h. After completion of the reaction, the reactor was cooled to room temperature. The reaction product was separated from the catalyst by filtration and the resulting product was analyzed using a GC-FID equipped with an Agilent HP-88 column. The results were calculated for the conversion and selectivity (Eqs. (1) and (2)).

$$Eth.Carb.Conv.(\%) = \frac{Init.Conct.\left(\frac{mol}{L}\right) - Final\ Conct.\left(\frac{mol}{L}\right)}{Init.Conct.\left(\frac{mol}{L}\right)} \times 100\% \quad (1)$$

$$Ethyl.Glycol\ Select.(\%) = \frac{Area\ of\ Ethyln.Glycol}{Total\ area\ all\ products} \times 100\% \quad (2)$$

3. Results and Discussion

The sol-gel method can be employed to efficiently produce silica from rice husks [15,16]. The process begins with the calcination of rice husks, which removes volatiles and water [17], resulting in the formation of the desired oxides. Subsequently, non-SiO_2 oxides were dissolved by leaching with 6 N HCl, improving both purity and surface area [18]. The dried samples were then dissolved in NaOH, which enabled the reaction between SiO_2 and NaOH to generate sodium silicate (Na_2SiO_3) [19]. The introduction of an acid to the sodium silicate solution triggers the condensation of silicate ions, transforming the siloxy groups (Si-O-) into silanol groups (Si-OH) and creating siloxane bonds (Si-O-Si), ultimately producing a white hydrogel [20]. The water content was reduced by drying at 110 °C for 12 h to evaporate surface water. XRF analysis revealed that the silica obtained from the rice husks had a purity of 96.1%.

The obtained silica was then used as a support in the synthesis of Cu-Ni/SiO_2 catalysts by varying the Cu:Ni ratios of 10:0, 7:3, 3:7, and 0:10 using the wet impregnation method. The obtained catalyst was calcined at 500 °C for 3 h to stretch the interpore space and improve the dispersion of metals on the support; thus, an active phase was formed, and contaminants were removed from the catalyst surface. The reduction of the metals using H_2 gas was then carried out in a tubular furnace at 550 °C for 4 h.

The X-ray diffraction (XRD) patterns shown in Figure 1 demonstrate the structural characteristics of the silica support derived from rice husks as well as the synthesized monometallic and bimetallic catalysts. The broad peak around 2θ = 21.7° in all diffractograms is indicative of amorphous silica, aligned with JCPDS #96-412-4080. This finding confirms that the rice-husk-derived silica predominantly exists in an amorphous form, with no crystalline silica phase being detected. Such amorphous silica can provide a favorable high-surface-area support for metal dispersion, contributing to catalytic

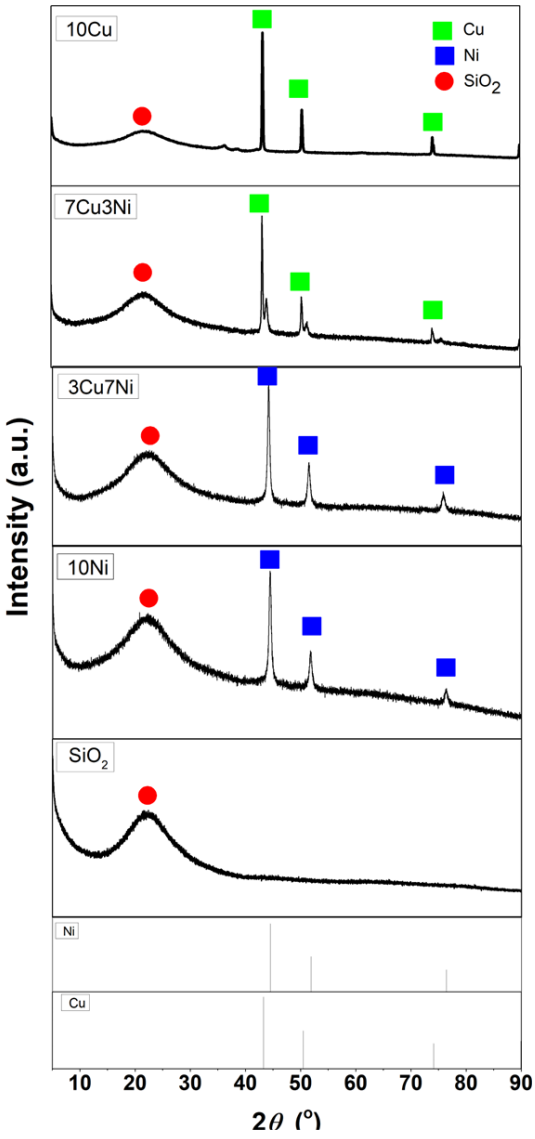

Figure 1. XRD patterns of the catalysts

performance. $10Cu/SiO_2$ exhibited sharp diffraction peaks at 2θ = 43.32°, 50.45°, and 74.11°, which correspond to the crystalline phases of metallic Cu (JCPDS #040836) [21]. These peaks indicated the presence of well-crystallized Cu particles on the silica support. Similarly, the $10Ni/SiO_2$ catalyst showed peaks at 2θ = 44.42°, 51.75°, and 76.35°, consistent with metallic Ni (JCPDS #01-1260) [22].

In the case of $7Cu3Ni/SiO_2$, the diffraction patterns revealed both Cu and Ni metal phases. This suggests that the Cu and Ni metals were well dispersed on the silica support, with no evidence of alloy formation or other significant phase interactions between the metals. For $3Cu-7Ni/SiO_2$, the Ni peaks dominate, reflecting a higher proportion of Ni in the bimetallic catalyst. The presence of both Cu and Ni phases in the bimetallic systems further suggests potential synergistic effects that could enhance the catalytic performance, as these structural characteristics can directly impact hydrogenation reactions, such as the transformation of ethylene carbonate to ethylene glycol. The prepared catalysts were characterized by X-ray fluorescence (XRF) to determine their constituent components. The XRF characterization results are presented in Table 1.

N_2 physisorption analysis provides valuable information regarding the surface area, pore volume, and pore size of the silica support and catalysts, contributing to a deeper understanding of their structural and catalytic properties. As detailed in Table 2, the silica derived from rice husks possesses a large surface area of 368.5 m^2/g, a pore volume of 0.72 cm^3/g, and an average pore size of 10.8 nm. These properties indicate that the silica support is mesoporous [23]. Mesoporous materials are crucial for catalysis because they provide an optimal balance between the surface area and pore size, facilitating the dispersion of metal particles and allowing for the efficient diffusion of reactants and products [24].

Upon impregnation of Cu and Ni into the silica support, significant changes in the surface area and pore size were observed, as seen in the properties of the synthesized catalysts. For example, the $10Cu/SiO_2$ catalyst showed a considerable reduction in the surface area (104.0 m^2/g) compared to the support, accompanied by an increase in the average pore size to 21.4 nm. This reduction in the surface area is attributed to the filling of the silica pores by Cu particles, which block the access to the inner surface of the support [25]. A similar trend is observed for the $7Cu3Ni/SiO_2$ catalyst, which exhibits a surface area of 99.6 m^2/g and a pore size of 21.4 nm, further confirming that metal impregnation reduces the number of available active sites on the silica surface by occupying the pore volume. Interestingly, the $3Cu7Ni/SiO_2$ catalyst has a higher surface area (258.0 m^2/g) than the other bimetallic catalysts, with a smaller average pore size of 10.7 nm. This suggests that a higher Ni content promotes better dispersion of metals on the silica surface, leaving a more accessible pore structure.

Furthermore, the $10Ni/SiO_2$ catalyst also showed a decrease in surface area (234.6 m^2/g) and a slight increase in pore size (12.1 nm) compared to pure silica. This pattern is consistent with the notion that metal impregnation leads to a reduction in the surface area because the metal particles partially block the mesopores of silica. However, the surface area of $10Ni/SiO_2$ remained relatively higher than that of $10Cu/SiO_2$, suggesting that Ni particles may not penetrate the silica pores deeply or may be more uniformly dispersed than the Cu particles.

The large surface area of the silica support enhances its ability to disperse metal particles, which is crucial for its catalytic activity. However, metal impregnation reduces the surface area and pore volume, which can affect the overall catalytic performance. Among the catalysts, $3Cu7Ni/SiO_2$ appears to maintain the best balance of surface area and pore size, which could be advantageous for catalytic reactions because it provides sufficient active sites, while maintaining a mesoporous structure that facilitates reactant and product diffusion. The smallest surface area of the $7Cu3Ni/SiO_2$ catalyst suggests that a higher Cu content leads to more significant pore blockage, which could negatively impact its catalytic performance by reducing the available active sites. These data indicate that the balance between the surface area and pore size plays a critical role in the performance of these catalysts.

Table 1. XRF analysis results

Catalyst	Amount (wt.%)	
	Cu	Ni
$10Cu/SiO_2$	15.0	-
$7Cu3Ni/SiO_2$	8.90	3.70
$3Cu7Ni/SiO_2$	4.40	9.30
$10 Ni/SiO_2$	-	12.70

Table 2. Pore properties of the catalysts

Catalyst	Surface Area (m^2/g)	Pore volume (cm^3/g)	Average pore size (nm)
SiO_2	368.5	0.72	10.8
$10Cu/SiO_2$	104.0	0.72	21.4
$7Cu3Ni/SiO_2$	99.6	0.56	21.4
$3Cu7Ni/SiO_2$	258.0	0.61	10.7
$10Ni/SiO_2$	234.6	0.61	12.1

The H_2-TPR profiles presented in Figure 2 provide valuable insights into the reduction behavior and metal-support interactions of both monometallic and bimetallic Cu-Ni catalysts supported on silica. The $10Cu/SiO_2$ monometallic catalyst exhibited a reduction peak at approximately 225 °C, which is notably lower than that of the $10Ni/SiO_2$ catalyst reduced at 335 °C [26]. This difference in reduction temperature is consistent with previous findings such as those reported by Gulyaeva *et al*. who indicated that Cu has a lower reduction temperature owing to its weaker interaction with the silica support [27]. In contrast, Ni exhibited a stronger interaction with the silica surface, making it more stable and requiring higher temperatures for reduction. This behavior emphasizes the higher reducibility and catalytic activity of Cu because a lower reduction temperature indicates that the catalyst is more readily activated for hydrogen dissociation, enhancing its efficiency in catalytic reactions involving hydrogenation.

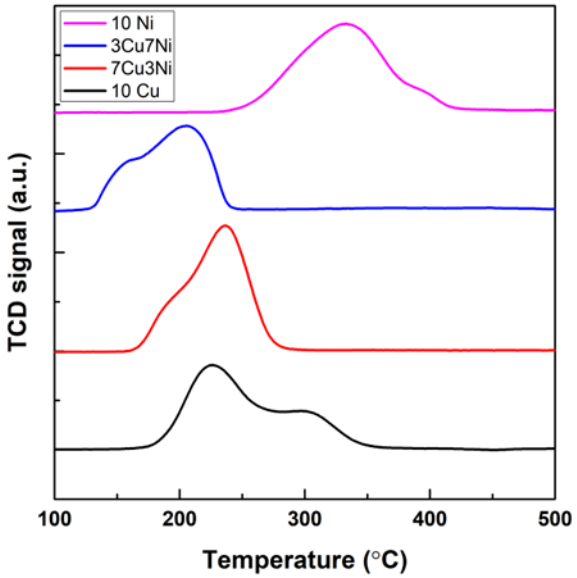

Figure 2. H_2-TPR profiles of the catalysts

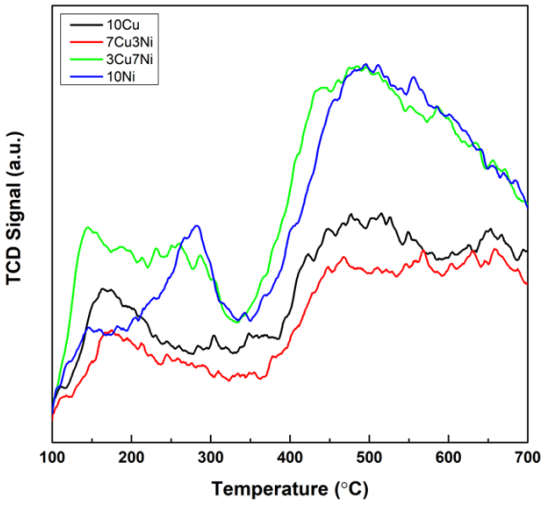

Figure 3. NH_3-TPD profiles of the catalysts

Bimetallic catalysts, particularly $7Cu3Ni/SiO_2$ and $3Cu7Ni/SiO_2$, show distinct reduction behaviors compared to their monometallic counterparts. The $7Cu3Ni/SiO_2$ catalyst exhibited a reduction peak at 237 °C, which was lower than that of the monometallic Ni/SiO_2 catalyst, but slightly higher than that of the $10Cu/SiO_2$ catalyst. This reduction temperature suggests that a Cu-rich bimetallic composition facilitates easier reduction than pure Ni, but retains some stability provided by the Ni component. In contrast, the $3Cu7Ni/SiO_2$ catalyst exhibited the lowest reduction temperature with a peak at 206 °C. This lower reduction temperature indicated enhanced reducibility, which could be due to the synergistic interaction between Cu and Ni in the catalyst. The strong interaction between Cu and Ni leads to a shift in the reduction temperature to a lower range (179-237 °C), demonstrating that the addition of Cu to Ni-based catalysts enhances their overall reducibility, making it easier to activate both metals during catalytic processes.

This synergistic effect is further evidenced by the relatively higher peak intensities observed for the bimetallic catalysts. The peak intensities indicate a cooperative reduction process between the NiO and CuO species on the silica surface, which enhances the overall reduction behavior of the catalyst. Specifically, the $3Cu7Ni/SiO_2$ catalyst displayed the lowest reduction peak, suggesting that it is highly reducible and may offer improved catalytic activity in hydrogenation reactions. The combination of Cu and Ni allows for a more efficient reduction process because Cu promotes the reduction of NiO, making it easier for both metals to participate in the catalytic process. This interaction between Cu and Ni not only enhances the reducibility of the catalyst but also contributes to its overall performance in reactions requiring active hydrogen dissociation.

NH_3-TPD analysis was performed to assess the acidic properties of the catalysts. Figure 3 and Table 3 present the results obtained from NH_3-TPD characterization. Figure 3 presents two key peaks for each catalyst: one at lower temperatures (below 350 °C), representing weakly acidic sites, and the other at higher temperatures (above 350 °C), indicating strongly acidic sites. The intensity and position of these peaks correlated well with the acidity values listed in Table 4, offering insights into the number and strength of acid sites across the different catalysts. $10Ni/SiO_2$ exhibited the highest total acidity (1.909 mmol/g), which corresponded to strong desorption peaks at higher temperatures, indicating the presence of stronger acid sites. In contrast, the $10Cu/SiO_2$ and $7Cu3Ni/SiO_2$ catalysts exhibited lower total acidity (1.110 mmol/g and 0.871 mmol/g, respectively) and weaker desorption peaks at

lower temperatures, suggesting weaker acid sites. This difference can be attributed to the distinct properties of the metals; Ni tends to form stronger Lewis acid sites because of its ability to generate robust metal-support interactions and coordinatively unsaturated sites that enhance surface acidity [28]. Furthermore, nickel ions, particularly Ni^{2+}, act as stronger electron acceptors than copper ions, which generally form weaker acidic sites [29]. The mixed metal catalyst $3Cu7Ni/SiO_2$ demonstrated moderate acidity (1.633 mmol/g) with a broad range of desorption temperatures, reflecting the synergistic effect of both metals, where nickel contributed stronger acidic sites, while copper modulated the overall acidity.

The SEM images (Figure 4) and EDX analysis (Table 4) of the Cu-Ni/SiO_2 catalysts provide valuable insights into the relationship between their morphology, elemental composition, and potential catalytic performance. The SEM images revealed distinct differences in the surface morphologies of the catalysts. The $10Cu/SiO_2$ catalyst displayed relatively large spherical particles, suggesting a well-defined but potentially lower surface area for catalytic reactions. In contrast, the combination of Cu and Ni in the $7Cu3Ni/SiO_2$ and $3Cu7Ni/SiO_2$ catalysts led to a more dispersed and granular morphology, particularly in $3Cu7Ni/SiO_2$, where finer, more homogeneous particles suggested an increased surface area and improved dispersion of metal species. The $10Ni/SiO_2$ catalyst showed smaller particles, consistent with the high surface area typically associated with Ni, which is known for its hydrogenation capabilities. In addition, $10Ni/SiO_2$, which had a high Ni content (16.6 wt. %) and small particle size, would be highly active in general hydrogenation processes, but may lack the selective properties of Cu in the catalyst. Among them, $3Cu7Ni/SiO_2$, with its balanced composition and fine dispersion, likely exhibited the best catalytic performance because of the optimal interaction between Cu and Ni, as suggested by the small, well-dispersed particles observed in the SEM image.

Table 3. Total acidity of the catalysts

Catalyst	Acidity (mmol/g)
$10Cu/SiO_2$	1.110
$7Cu3Ni/SiO_2$	0.871
$3Cu7Ni/SiO_2$	1.633
$10Ni/SiO_2$	1.909

Table 4. EDX analysis results

Catalyst	Amount (wt.%)	
	Cu	Ni
$10Cu/SiO_2$	7.2	-
$7Cu3Ni/SiO_2$	11.0	5.2
$3Cu7Ni/SiO_2$	5.7	6.0
$10Ni/SiO_2$	-	16.6

The EDX data complemented these observations by providing the elemental composition of each catalyst. For example, $10Cu/SiO_2$ contains 7.2 wt.% Cu and no Ni, indicating a pure copper catalyst supported on SiO_2. This composition, combined with the morphology, suggests moderate catalytic activity, as Cu is selective, but less active for hydrogenation reactions. However, the introduction of Ni into the $7Cu3Ni/SiO_2$ (with 11.0 wt.% Cu and 5.2 wt.% Ni) and $3Cu7Ni/SiO_2$ (5.7 wt.% Cu and 6.0 wt.% Ni) not only alters the morphology but also improves catalytic potential by promoting synergistic effects between the two metals. Ni enhances hydrogen activation, whereas Cu aids in selective hydrogenation, making these bimetallic catalysts particularly suited for reactions requiring both high activity and selectivity. Among them, $3Cu7Ni/SiO_2$, with its balanced composition and fine dispersion, is likely to exhibit the best catalytic performance because of the optimal interaction between Cu and Ni, as suggested by the small well-dispersed particles observed in the SEM image. In contrast, $10Ni/SiO_2$, which had a high Ni content (16.6 wt.%) and small particle size, would be highly active in general hydrogenation processes but may lack the selective properties that Cu brings to the catalyst.

The catalytic performance of Cu-Ni supported on rice husk-derived SiO_2 was evaluated in the conversion of ethylene carbonate to ethylene glycol. The conversion was performed in a batch reactor with an initial hydrogen pressure of 40 bar at 150 °C for 3 h. The hydrogenation of ethylene carbonate yields ethylene glycol and methanol as primary products and 1,2-propanediol and 1,2-butanediol as secondary products. Figure 5 presents the catalytic performance of the Cu-Ni/SiO_2 catalysts for the hydrogenation of ethylene carbonate into ethylene glycol, highlighting the differences in the conversion and selectivity of ethylene glycol. $10Cu/SiO_2$ demonstrated very low conversion (1.7%) with low ethylene glycol selectivity (15.1%), likely due to the ability of Cu to facilitate the hydrogenation process, but not as efficiently guide the selectivity towards ethylene glycol production. In contrast, $7Cu3Ni/SiO_2$ exhibited the best performance with 80.5% ethylene glycol selectivity, despite a modest ethylene carbonate conversion of 15.1%, implying an optimal synergy between Cu and Ni in enhancing selective hydrogenation. This could be attributed to the bimetallic nature of the catalyst,

where Ni enhanced hydrogen adsorption and activation, while Cu likely stabilized the intermediates, promoting ethylene glycol formation. In addition, electron transfer from Cu to Ni results in more stable Cu^{x+} species, allowing more Cu^0 sites to be released for hydrogen adsorption. The enhanced synergistic effect between Cu^0 and Cu^{x+} in the Cu-Ni/SiO_2 catalyst contributes to its excellent catalytic performance[30]. This indicates that the Ni metal incorporated into the Cu/SiO_2 catalyst causes Ni to be well dispersed to form a uniform Cu-Ni combination to enhance the adsorption and dissociation ability of H_2. The 3Cu7Ni composition further improved the ethylene carbonate conversion to 25.3% while maintaining a high ethylene glycol selectivity (74.2%), suggesting the dominant role of Ni in boosting the catalytic activity. Interestingly, the 10Ni catalyst showed the highest ethylene carbonate conversion (52.9%), but with slightly reduced ethylene glycol selectivity (54.4%), indicating that a Ni-rich environment favors ethylene carbonate hydrogenation, but at the expense of ethylene glycol selectivity, possibly due to over-hydrogenation or side reactions. These results suggest that the balance between Cu and Ni content plays a critical role in tuning the catalytic

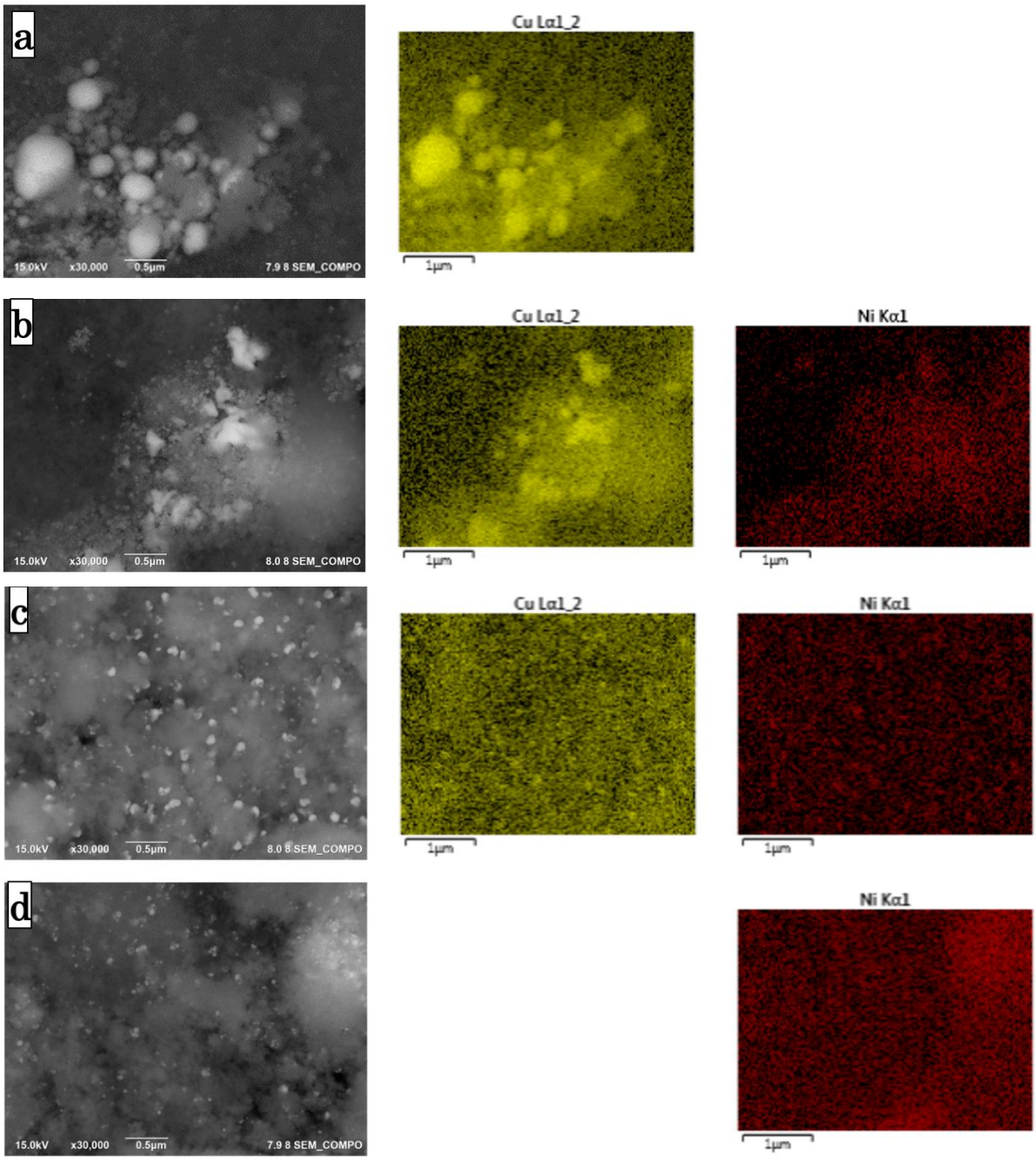

Figure 4. Surface morphology of the catalysts: (a) 10Cu/SiO_2, (b) 7Cu3Ni/SiO_2, (c) 3Ni7Cu/SiO_2, (d) Ni/SiO_2

properties, where Cu contributes to the selectivity and Ni contributes to the conversion efficiency. The superior performance of the 7Cu3Ni catalyst highlights the importance of controlling its metal composition to achieve the desired catalytic behavior.

4. Conclusions

Cu-Ni bimetallic catalysts supported on rice-husk-derived SiO_2 were successfully synthesized and characterized for the hydrogenation of ethylene carbonate to ethylene glycol. The catalysts exhibited varying degrees of performance depending on their Cu:Ni ratios. $7Cu3Ni/SiO_2$ demonstrated the best performance with 80.51% selectivity towards ethylene glycol, despite a modest ethylene carbonate conversion of 15.14%. This suggests an optimal synergy between Cu and Ni for enhancing selective hydrogenation. The balance between the Cu and Ni contents plays a critical role in tuning the catalytic properties. Cu contributed to the selectivity, whereas Ni enhanced the conversion efficiency. These findings highlight that while Cu primarily enhances selectivity, Ni contributes significantly to conversion efficiency, underscoring the critical role of fine-tuning the metal composition to optimize catalytic behavior. This study demonstrates the potential of Cu-Ni bimetallic catalysts supported on rice-husk-derived silica for the efficient and selective production of ethylene glycol from ethylene carbonate. Further research should focus on optimizing the reaction conditions and exploring the long-term stabilities of these catalysts to enhance their industrial applicability.

Acknowledgement

The authors declare that they have no competing financial interests or personal relationships that could influence the work reported in this study. The authors gratefully acknowledge the financial support provided by BRIN through the RP-ORNM 2024 program, LPDP through RIIM Batch 3 program, and KIST through the KIST Alumni Project Plus 2024.

CRedit Author Statement

Author Contributions: NSM: Investigation, Data Curation, Writing Draft Preparation; NDR: Writing; IA: Methodology, Investigation, Writing, Review and Editing, Supervision; YM: Validation, Writing, Review and Editing, Resources; EA: Validation; RRW: Validation, Resources; IY: Validation, Resources; JP: Validation; NR: Validation, Resources; AAD: Conceptualization, Methodology, Investigation, Resources, Data Curation, Writing, Review and Editing, Supervision, Project Administration, Resources. All authors have read and agreed to the published version of the manuscript.

References

[1] Robinson, P.R. Petrochemicals. In *Petroleum Science and Technology: Downstream*; Springer, 2024; pp. 243–291.

[2] Sharifara, E., Abbaspour, M., Saraei, A. (2024). Analysis of the High-pressure Steam Import Behaviour of an Integrated Ethylene Oxide/Ethylene Glycol Petrochemical Plant under Different Production Scenarios. *Can. J. Chem. Eng.* 102, 1538–1557. DOI: 10.1002/cjce.25143

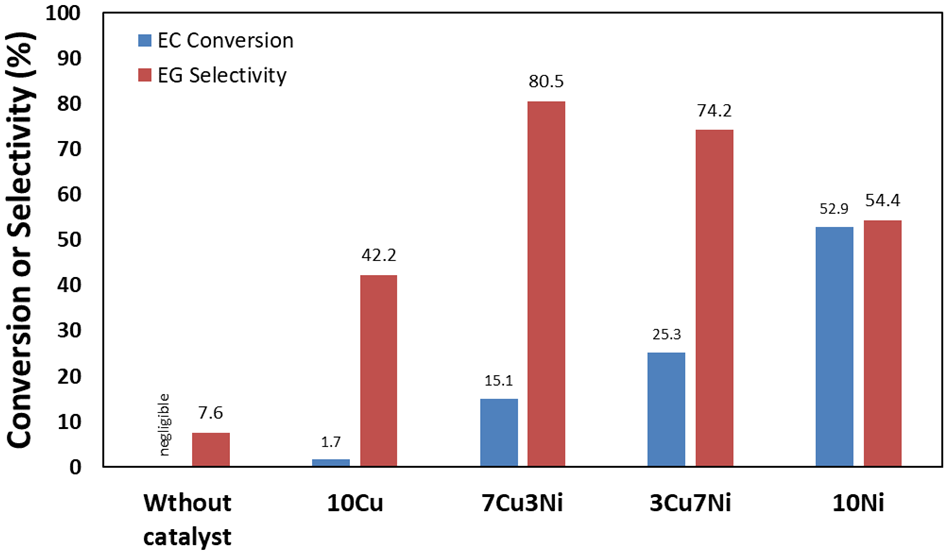

Figure 5. Catalytic activity of the catalysts

[3] Yang, Y., Yao, D., Zhang, M., Li, A., Gao, Y., Fayisa, B.A., Wang, M.-Y., Huang, S., Wang, Y., Ma, X. (2021) Efficient Hydrogenation of CO2-Derived Ethylene Carbonate to Methanol and Ethylene Glycol over Mo-Doped Cu/SiO2 Catalyst. *Catal. Today*, 371, 113–119. DOI: 10.1016/j.gce.2021.12.004

[4] Chen, X., Wang, L., Zhang, C., Tu, W., Cao, Y., He, P., Li, J., Li, H. (2021) The Effective and Stable Cu–C@ SiO2 Catalyst for the Syntheses of Methanol and Ethylene Glycol via Selective Hydrogenation of Ethylene Carbonate. *Int. J. Hydrogen Energy*, 46, 17209–17220. DOI: 10.1016/j.ijhydene.2021.02.166

[5] Riyandi, R., Rinaldi, N., Yunarti, R.T., Dwiatmoko, A.A., Simanjuntak, F.S.H. (2024) Effect of Various Silica-Supported Nickel Catalyst on the Production of Bio-Hydrocarbons from Oleic Acid. *International Journal of Renewable Energy Development*, 13, DOI: 10.61435/ijred.2024.60054.

[6] Zarib, N.S.M., Abdullah, S.A., Ishak, N.N. (2020) Extraction of Silica from Rice Husk and Bamboo Leaves and Its Effect on the Ceramic Body Glazing Process. *Applied Mechanics and Materials*, 899, 156–162, DOI: 10.4028/www.scientific.net/amm.899.156.

[7] Zhang, M., Yang, Y., Li, A., Yao, D., Gao, Y., Fayisa, B.A., Wang, M., Huang, S., Lv, J., Wang, Y. (2020) Nanoflower-like Cu/SiO2 Catalyst for Hydrogenation of Ethylene Carbonate to Methanol and Ethylene Glycol: Enriching H2 Adsorption. *ChemCatChem*, 12, 3670–3678. DOI: 10.1002/cctc.202000365

[8] Fayisa, B.A., Xi, Y., Yang, Y., Gao, Y., Li, A., Wang, M.-Y., Lv, J., Huang, S., Wang, Y., Ma, X. (2022) Pt-Modulated Cu/SiO2 Catalysts for Efficient Hydrogenation of CO2-Derived Ethylene Carbonate to Methanol and Ethylene Glycol. *Chin. J. Chem. Eng.*, 41, 366–373, DOI: 10.1016/j.cjche.2021.10.024.

[9] Liu, J., He, P., Wang, L., Liu, H., Cao, Y., Li, H. (2018) An Efficient and Stable Cu/SiO2 Catalyst for the Syntheses of Ethylene Glycol and Methanol via Chemoselective Hydrogenation of Ethylene Carbonate. *Chinese Journal of Catalysis*, 39, 1283–1293, DOI: 10.1016/S1872-2067(18)63032-3.

[10] Yang, Y., Zhang, J., Gao, Y., Fayisa, B.A., Li, A., Huang, S., Lv, J., Wang, Y., Ma, X. (2022) Highly Dispersed Nickel Boosts Catalysis by Cu/SiO2 in the Hydrogenation of CO2-Derived Ethylene Carbonate to Methanol and Ethylene Glycol. *Chin. J. Chem. Eng.*, 43, 77–85. DOI: 10.1016/j.cjche.2022.01.017

[11] Groß, A. (2006) Reactivity of Bimetallic Systems Studied from First Principles. *Top Catal.*, 37, 29–39, DOI: 10.1007/S11244-006-0005-X.

[12] Fayisa, B.A., Xi, Y., Yang, Y., Gao, Y., Li, A., Wang, M.Y., Lv, J., Huang, S., Wang, Y., Ma, X. (2022) Pt-Modulated Cu/SiO2 Catalysts for Efficient Hydrogenation of CO2-Derived Ethylene Carbonate to Methanol and Ethylene Glycol. *Journal of the Chemical Industry and Engineering Society of China*, 41, 366–373, DOI: 10.1016/j.cjche.2021.10.024.

[13] Gallego-Villada, L.A., Alarcón, E.A., Bustamante, F., Villa, A.L. (2024) One-Pot Tandem Catalysis: Green Synthesis of ß-Pinene Derivatives with MgO and Mesoporous Catalysts. *J. Catal.*, 438, 115698, DOI: 10.1016/j.jcat.2024.115698.

[14] Gallego-Villada, L.A., Mäki-Arvela, P., Kumar, N., Alarcón, E.A., Vajglová, Z., Tirri, T., Angervo, I., Lassfolk, R., Lastusaari, M., Murzin, D.Y. (2024) Zeolite Y-Based Catalysts for Efficient Epoxidation of R-(+)-Limonene: Insights into the Structure-Activity Relationship. *Microporous and Mesoporous Materials*, 372, 113098, DOI: 10.1016/j.micromeso.2024.113098.

[15] Shoodiqin, D.M., Musyarofah, M., Robiandi, F., Chairunnisa, R.C. (2024) Synthesis of Nano-Silica from Loa Kulu Rice Husk Using The Sol-Gel Method. *Indonesian Physical Review*, 7, 125–132, DOI: 10.29303/ipr.v7i1.280.

[16] Nehan, P.Z.Z., Akbar, A.A., Karim, M.I.N., Fahriza, R.A., Zainuri, M. (2023) Synthesis of Silica from Rice Husk Waste for Hydrophobic Material as an Anti-Water Coating for Eyeglasses. *Jurnal Fisika dan Aplikasinya*, 19, 44, DOI: 10.12962/j24604682.v19i2.15721.

[17] Shukla, S.K. (2020) Rice Husk Derived Adsorbents for Water Purification. In *Green Materials for Wastewater Treatment*; Naushad, Mu., Lichtfouse, E., Eds.; Springer International Publishing: Cham, pp. 131–148, ISBN 978-3-030-17724-9.

[18] Khalifa, M., Ouertani, R., Hajji, M., Ezzaouia, H. (2019) Innovative Technology for the Production of High-Purity Sand Silica by Thermal Treatment and Acid Leaching Process. *Hydrometallurgy*, 185, 204–209, DOI: 10.1016/j.hydromet.2019.02.010.

[19] Febriana, E., Mayangsari, W., Yudanto, S.D., Sulistiyono, E., Handayani, M., Firdiyono, F., Maksum, A., Prasetyo, A.B., Soedarsono, J.W. (2024) Novel Method for Minimizing Reactant in the Synthesis of Sodium Silicate Solution from Mixed-Phase Quartz-Amorphous SiO2. *Case Studies in Chemical and Environmental Engineering*, 9, 100656, DOI: 10.1016/j.cscee.2024.100656.

[20] Geddes, C.D., Birch, D.J.S. (2000) Nanometre Resolution of Silica Hydrogel Formation Using Time-Resolved Fluorescence Anisotropy. *J. Non Cryst. Solids*, 270, 191–204, DOI: 10.1016/S0022-3093(99)00962-X.

[21] Mahanti, M., Basak, D. (2014) Cu/ZnO Nanorods′ Hybrid Showing Enhanced Photoluminescence Properties Due to Surface Plasmon Resonance. *J. Lumin.*, 145, 19–24. DOI: 10.1016/j.jlumin.2013.07.028

[22] Wang, Y., Li, H., Ren, Y., Chen, X., Xie, K., Sun, Y. (2018) Nanowire-Core/Double-Shell of NiMoO4@ C@ Ni3S2 Arrays on Ni Foam: Insights into Supercapacitive Performance and Capacitance Degradation. *Nanotechnology*, 29, 385402. DOI: 10.1088/1361-6528/aad0b5

[23] Shelke, V.R., Bhagade, S.S., Mandavgane, S.A. (2010) Mesoporous Silica from Rice Husk Ash. *Bulletin of Chemical Reaction Engineering & Catalysis*, 5, 63–67. DOI: 10.9767/bcrec.5.2.793.63-67

[24] Yu, X., Williams, C.T. (2022) Recent Advances in the Applications of Mesoporous Silica in Heterogeneous Catalysis. *Catal. Sci. Technol.*, 12, 5765–5794. DOI: 10.1039/D2CY00001F

[25] Vasiliadou, E.S., Eggenhuisen, T.M., Munnik, P., De Jongh, P.E., De Jong, K.P., Lemonidou, A.A. (2014) Synthesis and Performance of Highly Dispersed Cu/SiO2 Catalysts for the Hydrogenolysis of Glycerol. *Appl. Catal. B Env.*, 145, 108–119. DOI: 10.1016/j.apcatb.2012.12.044

[26] Wang, F., Han, K., Xu, L., Yu, H., Shi, W. (2021) Ni/SiO2 Catalyst Prepared by Strong Electrostatic Adsorption for a Low-Temperature Methane Dry Reforming Reaction. *Ind. Eng. Chem. Res.*, 60, 3324–3333. DOI: 10.1021/acs.iecr.0c06020

[27] Gulyaeva, Y., Alekseeva, M., Bulavchenko, O., Kremneva, A., Saraev, A., Gerasimov, E., Selishcheva, S., Kaichev, V., Yakovlev, V. (2021) Ni–Cu High-Loaded Sol–Gel Catalysts for Dehydrogenation of Liquid Organic Hydrides: Insights into Structural Features and Relationship with Catalytic Activity. *Nanomaterials*, 11, 2017, DOI: 10.3390/nano11082017/S1.

[28] Wang, Y., Zhang, Z., Zhang, S., Wang, Y., Hu, S., Xiang, J., Wei, T., Niu, S., Hu, X. (2022) Correlations of Lewis Acidic Sites of Nickel Catalysts with the Properties of the Coke Formed in Steam Reforming of Acetic Acid. *Journal of the Energy Institute*, 101, 277–289, DOI: 10.1016/j.joei.2022.02.006.

[29] Sharma, S.K., Hundal, G., Gupta, R. (2010) The Effect of Ligand Architecture on the Structure and Properties of Nickel and Copper Complexes of Amide-Based Macrocycles. *Eur. J. Inorg. Chem.*, 2010, 621–636, DOI: 10.1002/EJIC.200900623.

[30] Chen, W., Song, T., Tian, J., Wu, P., Li, X. (2019) An Efficient Cu-Based Catalyst for the Hydrogenation of Ethylene Carbonate to Ethylene Glycol and Methanol. *Catal. Sci. Technol.*, 9, 6749–6759, DOI: 10.1039/C9CY01586H.